Probing the quark gluon plasma medium through B meson production measurements in PbPb collisions at the LHC

Júlia Manuela Cardoso Silva
juliasilva@tecnico.ulisboa.pt

Instituto Superior Técnico, Lisboa, Portugal

October 2019

Abstract

Relativistic heavy ion collisions allow the study of Quantum Chromodynamics at high energy density and temperature. Under such conditions, a medium of deconfined quarks and gluons is predicted to be formed, the Quark-Gluon Plasma (QGP). Heavy quarks are produced in the early stages of heavy ion collisions, experiencing the full evolution of the QGP medium, losing energy in their interactions with the medium before hadronising. Exclusive beauty production measurements add precision to the study of parton energy loss and allow to probe its flavour dependence. An enhancement in strangeness content is expected in the probed medium. If beauty hadronisation happens through quark-recombination in the QGP, B_s production is expected to be larger than B^+ production. B mesons are novel probes of the QGP, and only recently have they been reconstructed in nuclear collisions. This work employs data collected by the Compact Muon Solenoid, in PbPb collisions with a center-of-mass energy of 5.02 TeV, at the Large Hadron Collider. The first observation of B_s in PbPb is presented, with a significance over 5σ. B_s and B^+ cross sections are measured as a function of transverse momentum (p_T) and centrality. The ratios between the two are computed and compared to the fragmentation fraction ratio f_s/f_u, measured in pp collisions. Evidences of bottom hadronisation through recombination in the medium are shown for low B p_T and more central collisions. Using the published B_s cross sections in pp collisions, in the p_T range of 15-50 GeV/c, the B_s nuclear modification factor is computed. The measurements indicate an overall suppression of B_s production in the QGP medium, in the probed kinematic region.
Keywords: Quark Gluon Plasma, Compact Muon Solenoid, B Physics, Heavy Ion Collisions, Cross Section

1. Introduction

For high energy densities and temperatures, a medium of deconfined quarks and gluons is predicted, the quark-gluon plasma (QGP) [1]. This medium is created in relativistic heavy ion collisions. However, it is short-lived and consequently it cannot be accessed directly. Experimenters use different probes, allowing the measurement of medium effects.

1.1. Heavy Flavour Probes of the QGP

Heavy flavour quarks (namely charm and beauty quarks) are abundantly produced at the LHC and are particularly interesting as probes of the QGP medium giving us insight into its underlying mechanisms. These quarks are produced in the early stages of the heavy ion collisions, in hard scattering processes between partons of the incoming nuclei [3]. Because of their large masses, higher than QGP's critical temperature[1] ($M_{c,b} > T_c$), their production time is shorter than the formation time of QGP. Given that their thermal production and annihilation rates are negligible, heavy quarks experience the full evolution of the QGP medium.

A dependence on quark flavour is predicted for radiative energy loss in the QGP medium: the so-called "dead cone effect" [2]. This effect arises from increasing suppression of medium induced gluon radiation, for higher mass quarks. Notwithstanding, for high enough quark energies, this effect should cease. The study of hadrons of different flavours and masses should facilitate an understanding of such dependences of the underlying energy loss mechanisms in the medium.

It was theoretically proposed that strangeness production in the QGP medium would be enhanced in comparison to a hadron gas. That should be consequence of the high rate of the process $gg \to s\overline{s}$, if the medium's temperature is above the strange quark mass [9]. Furthermore, it was also suggested that low-momentum heavy quarks could

[1] Temperature of transition to the quark gluon plasma state.

hadronise via recombination with other quarks in the QGP [3]. If recombination in the medium is significant, one should expect to observe less suppressed strange D and B mesons with respect to lighter mesons of the same kind, in face of the medium with an increased strangeness content.

1.2. B mesons

B mesons are comprised of two quarks - a bottom antiquark and a quark of a different flavour. Depending on that second quark we can have a B^+ ($\bar{b}u$), B^0($\bar{b}d$), B_s ($\bar{b}s$) or a B_c ($\bar{b}c$). In this work the main focus was on B^+ and B_s. Charge conjugated states are implied unless otherwise specified.

After being produced, single bottom quarks hadronise with a quark of different flavour with different probabilities, called b fragmentation fractions f_X, where X denotes the flavour of the second quark of the formed B meson. LHCb has measured the ratios $f_s/(f_u + f_d)$ in pp collisions [13], and investigated its dependence on transverse momentum. If one assumes that because of isospin symmetry, the probability of hadronization of a b quark into a B_s or a B^+ meson will be the same, $f_u = f_d$ and $f_s/(f_u + f_d) = f_s/2f_u$. The independent inclusive (i.e. for the entire range of p_T) measurements of f_s/f_d and $f_s/(f_u + f_d)$ are compatible with this assumption, within uncertainty values.

B mesons decay via the weak interaction. The more massive $\bar{b}$ is usually the one that decays, the dominant decay being $\bar{b} \rightarrow \bar{c}W^+$. The virtual W boson will then materialise into a pair of leptons or quarks which hadronise thereafter. The probability of a particle decaying into a specific final state out of all possible final states is referred to as a branching fraction ($\mathcal{B}$). B mesons have a long lifetime, travelling a measurable distance in the detector. They are then said to produce a "displaced vertex". The B^+ production was studied in this analysis through the decay channel $B^+ \rightarrow J/\psi(\mu^+\mu^-)K^+$, while the B^s production was studied through $B_s \rightarrow J/\psi(\mu^+\mu^-)\phi(K^+K^-)$.

1.3. Production Measurements

B meson production measurements can be a window to gaining information about the QGP, allowing to probe it for the effects already mentioned. In practise, production is quantified by a cross-section. One can perform an inclusive measurement, or if there is the intent of exploring a possible dependence to a specific kinematic variable, a differential measurement can be done. The differential cross section in transverse momentum (p_T), for a given B meson, explored through a specific decay channel, can be computed by [5]:

$$\frac{d\sigma(\overline{B})}{dp_T} = \frac{1}{2}\frac{N}{\mathcal{A}\epsilon\mathcal{B}\mathcal{L}\Delta p_T}, \quad (1)$$

where N represents the raw yield extracted in an analysis, $\mathcal{A}$ is the detector's acceptance, ϵ the efficiency associated with the performed analysis, $\mathcal{B}$ is the branching fraction of the decay channel used, $\mathcal{L}$ the integrated luminosity, that is a measurement of the collected data size (in units of inverse area). The factor of 2 accounts for the fact that the measure is done for both particle and antiparticle.

When studying the QGP effects on B meson production, one further computes the nuclear modification factor (R_{AA}), a ratio between the production in nucleus-nucleus (σ_{AA}) and pp (σ_{pp}) collisions, scaled by the expected number of binary collisions [1],

$$R_{AA} = \frac{1}{\langle N_{coll}\rangle}\frac{\sigma_{AA}}{\sigma_{pp}}. \quad (2)$$

If $R_{AA} < 1$ it is said that the medium caused suppression, and for $R_{AA} > 1$ the opposite effect of enhancement.

1.4. State of the Art

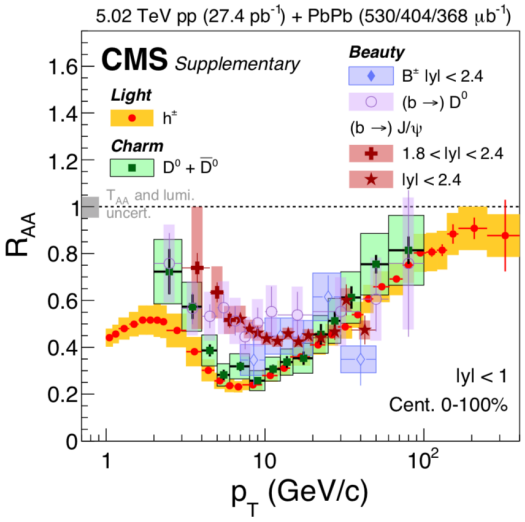

Figure 1: Nuclear modification factors of different hadrons, measured in PbPb collisions at $\sqrt{s}$ =5.02 TeV, as a function of transverse momentum. Results obtained by the CMS Collaboration [3].

The flavour dependence of energy loss in QGP has been tested by comparing the nuclear modification factors of different hadrons [3]. Figure 1 shows the results obtained by CMS in function of p_T of the hadron. This comparison is performed between: light charged hadrons ($h^{\pm}$), i.e. kaons and pions; prompt D^0, i.e., D^0 not coming from the decays of heavier particles; non-prompt D^0, i.e., D^0 coming from the decays of b hadrons; non-prompt J/ψ, i.e. J/ψ coming from b hadron decays; and $B^{\pm}$ mesons. For low p_T light charged hadrons are more suppressed than open heavy flavour hadrons. In addition, at intermediate p_T, the nuclear modification factor of non-prompt J/ψ

is significantly higher than for D^0, supporting a bottom-charm hierarchy. That difference is reinforced when one is reminded that non-prompt J/ψ does not carry the full p_T of the B meson that generated it, so a shift for slightly higher p_T should be accounted for when doing the comparison. At high p_T there is a degeneracy of the R_{AA}'s. This is expected, since the energy-to-mass ratio becomes large, and so the mass effects should cease. It is also seen that the degeneracy of light-charm hadrons R_{AA} happens at around 10 GeV/c, and bottom R_{AA} further degenerates at around 25 GeV/c.

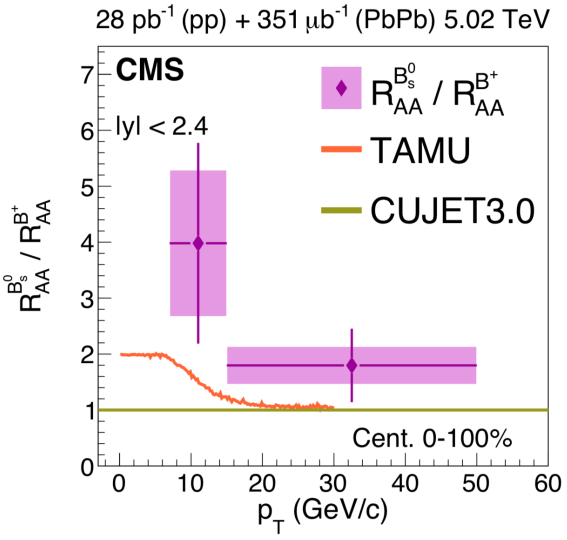

Figure 2: B_s and B^+ nuclear modification factor ratios, in PbPb collsions at CMS [3].

Also, the enhancement of strange heavy flavour mesons relative to their non-strange counterparts has been probed in heavy ion collisions. Using 2015 data from PbPb collisions at 5.02 TeV, B_s production results have been recently published by CMS. Its ratio relative to B^+ has also been presented (Figure 2) [11]. The data seems to suggest an enhancement relative to the B^+ case. However, the B_s signal is not sufficiently significant in the analysed dataset, and there are large statistical uncertainties affecting the comparison. A more precise measurement must be performed, offering more insight on hadronisation in the bottom sector.

In November 2018, a larger dataset was collected by CMS with the LHC running for PbPb collisions. The data sample is larger by a factor of 3, comparatively to the one used for the analysis that yielded Figure 2. The larger dataset will be employed for this analysis. B mesons are novel probes of the QGP, since only in the last few years has their exclusive measurement been possible in this medium. This means that one can fully reconstruct a specific B decay channel, reconstructing its identity and kinematics. The first observation of the B_s signal in PbPb collisions will result in a robust quantification of the competing medium effects of suppression and enhancement, relative to the B^+.

2. Experimental Framework

The Large Hadron Collider (LHC) can be found in a 27 km circular tunnel and it has been performing pp and PbPb collisions at the highest energies over the past years. Protons/nuclei go through a series of accelerators before being injected into the LHC ring in the form of two counter-rotating beams, where they are further accelerated to their nominal energies. The counter-rotating beams are brought into collision in 4 interaction points where 4 main detectors are located. One of those detectors is the Compact Muon Solenoid (CMS). Its central feature is a 13 m long, 6 diameter superconducting solenoid, that creates a magnetic field of around 3.8 T. It is composed of subdetectors that are arranged cylindrically around the beam pipe. In Figure 3 a transverse slice through CMS is displayed, showing its layers. From the beam to outside one finds: the silicon tracker, electromagnetic and hadron calorimeters, the solenoid, and the muon chambers. Different particles will deposit their energy at different parts of the detector. Photons and electrons will stop at the electromagnetic calorimeter, and hadrons will stop in the hadron calorimeter. Except for neutrinos, that are not detected, only muons get to the last layer, because they do not interact strongly and are too massive to emit a substantial fraction of energy through electromagnetic radiation, being able to penetrate dense materials, like steel. The most relevant sub-detectors, for this work, are the silicon tracker (measures the trajectories of charged particles, "tracks"), and the muon stations (measures the trajectory of the muons that manage to reach it). The hadron calorimeter also plays a key role for this analysis, since centrality is estimated from energy deposits in the hadron forward calorimeters (HF). This is an important quantity for nucleus-nucleus collisions, since it quantifies the extent of the overlap between the two colliding nuclei (0% being the most overlap). Experimentally, one uses the distribution of the total transverse energy deposited in the HF, to divide an event sample into centrality classes. For instance, the top 10% most energy deposited corresponds to a centrality class of 0–10%.

Only a small fraction of the collisions that occur at the interaction point will contain physics processes of interest to each analysis. Furthermore, the storage space and rate of data transfer required make it impossible to keep a record of all the collision events. As a result, a trigger system is crucial to select only the interesting fraction of the events.

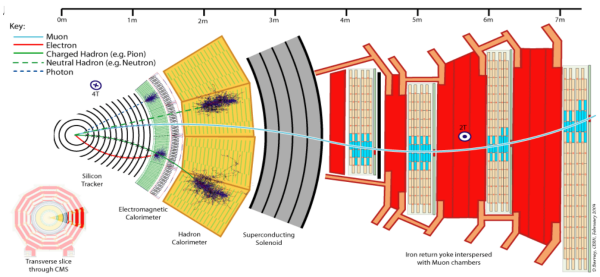

Figure 3: Transverse view of the CMS detector, showing its different layers.

The CMS trigger system is divided into two decision levels: level one (L1) trigger, and high-level trigger (HLT) [6].

3. Data, Monte Carlo Samples and Selection

This analysis was performed using data from the 2018 PbPb run, with a center-of-mass energy of $\sqrt{s_{NN}} = 5.02$ TeV, and corresponding to a total integrated luminosity of 1.5 nb^{-1}. The trigger employed required the presence of two muon candidates, since for both decays of interest there are two muons in the final state. Monte Carlo (MC) simulations are key for particle physics analysis, since they allow access to the correspondence between a physics process and detector signatures. They are used in this work in several steps of the analysis, but most importantly for acceptance and efficiency calculations.

The B meson reconstruction procedure takes advantage of the long decay length of these particles, that produce what is called a displaced vertex in the CMS detector. This displacement exists between the point where the nucleon collision occurred (Primary Vertex) and the point where the B mesons decayed (Secondary Vertex). For each event, combinations of tracks (the kaons in these case) and muons are fitted together, reconstructing one, or more[2] secondary vertices, displaced from the corresponding primary vertices. Basic kinematic and quality selections are applied to both muons and tracks. Two muons with an invariant mass within 0.15 GeV/c^2 of the J/ψ mass are fitted together with a common vertex constraint to reconstruct J/ψ candidates. For the B_s, tracks are also fitted together (with an invariant mass within 0.015 GeV/c^2 of the ϕ mass), forming ϕ candidates. The J/ψ candidates are then fitted with the ϕ candidates, forming a B_s candidate. In the case of B^+, J/ψ candidates are fitted together with the K^+.

Both B_s and B^+ candidates are further selected based on the χ^2 probability of their decay vertex (the probability for the muon tracks from the J/ψ meson decay and the other charged particle tracks to originate from a common vertex), the decay length (normalized by their uncertainties), the pointing angle (the angle between the line segment connecting the primary and decay vertices and the momentum vector of the B meson), the cosine value of the angle between B mesons displacements and momenta in the transverse direction, the 2D distance between the primary and decay vertices of their daughter tracks (normalized by their uncertainties) and the p_T of the daughter charged tracks.

For B_s, the z direction distance between the primary and decay vertices of their daughter tracks (normalized by their uncertainties) and the distance of the two hadronic tracks' invariant mass to the ϕ meson resonance are also used as selection variables. These variables are combined via multivariate discriminators, based on a boosted decision tree (BDT) implementation [10]. The BDT training is performed by employing simulated B signal samples and background samples taken from data sidebands (candidates with invariant mass 0.20–0.30GeVc^2 away from the B mesons' mass [12]). The selection is optimized separately for each meson, as well as each individual bin of p_T. The chosen requirement of the BDT score is the one that maximises $S/\sqrt{S+B}$, where S is the number of signal candidates in signal region after applying a given cut to the BDT, while B is the number of background candidates in the signal region after applying that same cut.

The analysis was performed in the fiducial region given by: $|y| < 1.5$, $p_T > 10$ GeV/c; $1.5 < |y| < 2.4$, $5 < p_T < 60$ GeV/c, for the B^+; $|y| < 1.5$, $p_T > 10$ GeV/c; $1.5 < |y| < 2.4$, $7 < p_T < 50$ GeV/c, for the B_s.

4. Signal Extraction

The raw B meson signal yields are extracted using an extended unbinned maximum likelihood fit to the invariant mass spectra. The signal shapes are modelled by two Gaussian functions, with parameters determined from MC simulation. The combinatorial background, from uncorrelated combinations of tracks and muons, gives rise to a falling contribution in the invariant mass spectrum which is modelled by an exponential function. An additional background source can arise from possible contaminations of other B hadron decays. For the B^+ spectrum, partially reconstructed B decays, for instance $B_s \to J/\psi\, K^+K^-$, where one kaon (K^-) is missed, lead to a heightened background in the invariant mass region below 5.2 GeV/c^2. The decay $B \to J/\Psi\pi^+$, where the pion is misidentified as a kaon, results in a small peaking structure under the signal peak. Such partially and mis-reconstructed B hadron components are modelled from simula-

[2] There can be more than one B meson candidate for each event!

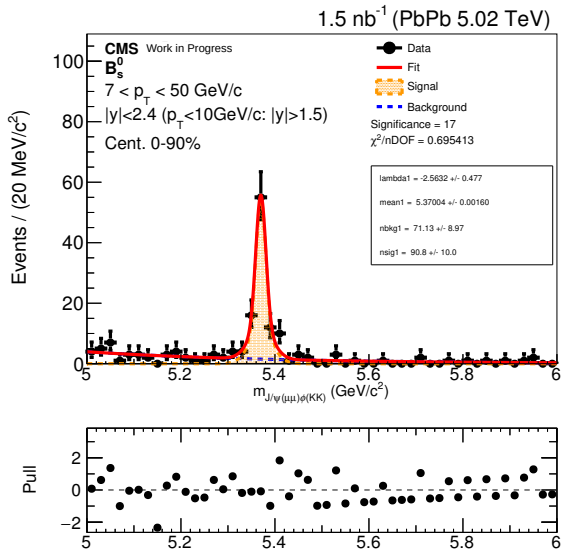

Figure 4: B_s meson invariant mass fit in data. nsig1 and nbkg1 are the number of signal and background candidates, lambda1 is the exponential decay slope and mean1 is the mean of the gaussian. Below the fit, the pull histogram is displayed.

tion, via an error function and a Gaussian function, respectively; both shapes and the Gaussian normalisation (relative to the signal) are fixed in the fit to the data. For the B_s case, such background contributions are found to be negligible, as a consequence of the tight selection on the mass of the ϕ candidate. The fit to the B_s invariant mass spectra is shown in Fig. 4. The statistical significance of the B meson signals is estimated from the ratio of likelihoods obtained by fitting the data with the full model and the background-only model. Estimates in excess of 51 and 17 standard deviations are thus obtained for the B^+ and B_s mesons, respectively.

5. Acceptance and Efficiency

Not all B mesons can be measured by the analysis. First, because of the detector design and positioning, not all particles generated by the collisions can be detected. For instance, the muon chambers were positioned in CMS in the $|\eta|$ <2.4 region, so muons with $|\eta|$ >2.4 (possibly coming from B meson decays here studied) will not be detected. The acceptance is here defined as the fraction of generated B mesons (in the fiducial region) that produced tracks and muons that lie within the detector's geometrical constrains. In order to observe a peak in the B meson invariant mass, optimised selection was applied to the data. There might have been signal candidates that did not pass all the requirements. Also the B meson reconstruction process must result in some fraction of the signal candidates lost. The efficiency is here defined as the fraction of generated B mesons within the acceptance region of the detector, with daughters that survived their individual selection requirements, and that were correctly reconstructed and survived all the selection requirements. The acceptance and efficiencies calculations are done using the Monte Carlo samples, producing 2-dimensional fine-grained maps of acceptance and efficiency as functions of B p_T and y.

To account for discrepancies between data and MC regarding muon selection and identification, the tag and probe method was employed to provide scaling factors that are applied to the 2D maps. The fundamental idea of TnP is to reconstruct a well-known resonance built on two objects. In this case, the interest is on muon efficiency so the resonance may be, for instance, the Z or J/ψ particle. This resonance is built on two muons, of which one will be called the "tag" and the other the "probe". Tag muons are required to meet tight selection criteria, so they will almost certainly be muons. On the other hand, probe muons are selected with a very loose set of criteria, that introduces very little bias. The probe objects are the ones that will be used to examine the efficiency of some specific selection criteria. A probe muon is matched with a tag muon such that the invariant mass of the formed dimuon is consistent with the mass of the chosen resonant peak. Through this matching with tag muons, one assures that probe muons are almost likely true muons. Two invariant mass distributions are formed: "passing probes" and "failed probes", according to whether or not the probe meets the selection criteria for which the efficiency is being estimated. The resulting mass peaks are fitted and the yields (N) can be used to calculate the measured efficiency for a specific selection. The efficiencies of muon trigger (ϵ_{trg}), track reconstruction (ϵ_{trk}), and identification (ϵ_{muid}) were calculated by the CMS dilepton group in this way. Comparing the results obtained from the TnP method in data and MC, the discrepancy can be estimated, and the scaling factors to be applied to the 2D efficiency maps.

From the fine-grained 2D maps one can read a $\alpha \times \epsilon$ value for each candidate in data, with specific p_T and y values. Then, for each p_T range used in the analysis (Δp_T), one averages over the candidates in the signal region, obtaining a p_T and rapidity dependent $\langle 1/(\alpha \times \epsilon) \rangle$ for each p_T bin. The results are shown in Figure 5, for B_s.

6. Data-MC Comparison

The signal MC simulation is validated against data by inspecting the distributions of the variables employed in the selection. The signal distributions are extracted from the data employing the SPlot method [8], and are also cross-checked with the alternative sideband-subtraction method. The SPlot

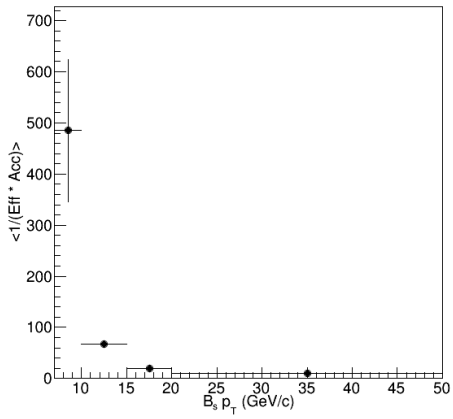

Figure 5: Product of B_s meson acceptance and efficiency as a function of p_T within 0-90% centrality. The TnP scaling has already been applied.

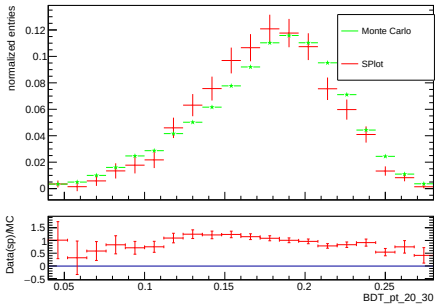

Figure 6: Comparison of B^+ BDT score (trained in the p_T bin of 20-30 GeV/c) distribution in data (obtained through SPlot) and MC.

method uses the B invariant mass as a discriminating variable, and employs an extended maximum likelihood fit for its modelling. From that fit candidate-by-candidate weights are computed, representing the probability of a candidate belonging to either the signal or background component. the wights can be applied to data distributions, providing individual signal and background distributions.

The sPlot-derived distributions for the BDT score are retrieved from the data, along with corresponding data/MC ratios, that are used in the estimation of the uncertainties on the efficiency calculations. Figure 6 shows one of the obtained comparisons. The bottom panel shows the ratios to be used in systematic uncertainties calculations.

7. Systematic Uncertainties

The cross section measurements are affected by several sources of systematic uncertainties arising from the signal extraction, acceptance and efficiency. Uncertainties on the normalisation factors to be used in the final cross section calculation are also propagated as systematic uncertainties on the final result.

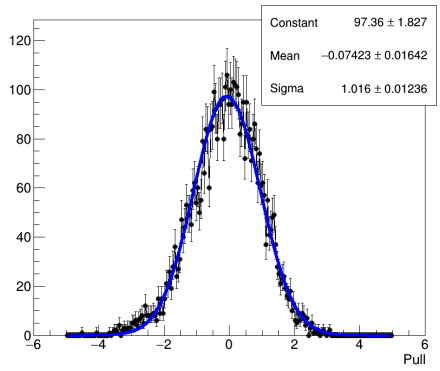

Figure 7: Pull distribution obtained from toy MC study, in the case of B_s.

The uncertainty from signal and background modeling is evaluated by considering four fit variations: (i) using low-order polynomials for describing the combinatorial background, (ii) using a sum of three Gaussian functions with a common mean for describing the signal, (iii) fixing the mean of the Gaussian function to the value determined from simulation; (iv) releasing the MC-based constraint on the width of the signal double Gaussian, by allowing a resolution scale factor to float in the fit. The maximum of the signal variations and the maximum of the background variations are propagated as systematic uncertainties.

Another systematic uncertainty associated with the signal extraction procedure arises if there is a bias in the modelling. By definition, the fit procedure is unbiased if it yields, on average, the correct value for the parameter of interest, in this case, the number of signal events. This was tested through a pseudo-experiments study. 5000 pseudo-data samples were generated, according to the resulting PDF from the fits done during the signal extraction procedure. Each sample of pseudo-data was then fitted with the same model used in the data fittin, and the pull distributionwais evaluated. The pull distribution is expected to be a Gaussian with mean equal to 0 and standard deviation equal to 1. Deviations from null mean will be propagated as the systematic uncertainty associated with fit bias. The produced pull distribution for B_s can be found in Figure 7. The deviations to null mean are multiplied by the statistical uncertainty of the signal yield of the corresponding fit to data. The obtained value is further divided by the signal yield, to obtain a relative systematic uncertainty. This estimation was only done for the full datasets of either B^+ or B_s.

The data-MC ratios obtained from the SPlot method are used to re-weight the MC simulation, and the resulting deviation in the $\langle 1/\alpha \times \epsilon \rangle$ factors are assigned as the systematic uncertainties. This procedure is employed using the higher-yield chan-

nel, namely the B^+. For the B_s meson, the limited size of the data sample yields results that are generally compatible between data and simulation, within the statistical uncertainties. As such, the B^+ channel is used as calibration mode for the B_s channel, given the similar decay topologies. A procedure identical to that described above, applied to the B^+ sample, is employed but using only tracking related variables. The systematic uncertainty for the B_s corresponds to that evaluated for the B^+ and further adding in quadrature the deviation determined from tracking related variables.

The systematic uncertainties associated with the TnP method are propagated as systematic uncertainty on the $\langle 1/\alpha \times \epsilon \rangle$ factors. The difference in the track reconstruction efficiency in data and simulation was estimated studying the $D^* \to \pi\pi(\pi\pi)$ decays [4], and results in 5% (10%) uncertainty in the efficiency determination for the B^+ (B_s) decay for involving one (two) kaons.

8. Results & Discussion

The cross section was finally computed for the analysis fiducial region through:

$$\frac{d\sigma^B}{dp_T} = \frac{1}{2\,\mathcal{B}\,N_{\text{MB}}\,T_{AA}} \frac{N_{\text{obs}}(p_T)}{\Delta p_T} \left\langle \frac{1}{\alpha(p_T,y)\cdot\epsilon(p_T,y)} \right\rangle . \quad (3)$$

The normalisation was here performed with the nuclear overlap function (T_{AA}) multiplied by the number of minimum bias events (N_{MB}). The T_{AA} is equal to the number of nucleon-nucleon (NN) binary collisions divided by the NN total inelastic cross section, and it can be interpreted as the NN-equivalent integrated luminosity per heavy ion collision. It is estimated by Glauber Model simulation [7]. The normalisation was not done with luminosity, like it is standard in pp collision measurements due to higher uncertainties associated with the luminosity in PbPb collisions.

p_T and centrality differential cross section measurements were performed within the fiducial region for both B^+ and B_S . Figure-8 shows the p_T differential results obtained for B_s, as an example. The dominant systematic uncertainty is the one arising from data-MC disagreement.

The B_s/B^+ production rations were computed through

$$R = \frac{N_{\text{obs}}^{B_s}}{N_{\text{obs}}^{B^+}} \frac{\langle 1/\alpha^{B_s}\epsilon^{B_s}\rangle}{\langle 1/\alpha^{B^+}\epsilon^{B^+}\rangle} \frac{\mathcal{B}^{B^+}}{\mathcal{B}^{B_s}} . \quad (4)$$

The normalisation factors are no longer a source of systematic uncertainty, since they cancelled in the division. Given the similar topology of the decay channels, systematics related to the efficiency determination cancel in first order. The systematics associated with muon efficiency (coming from the application of the tag and probe technique) are then neglected for the ratio. Since the only difference in the final state of the two decay channels is the presence of an extra track for B_s, only uncertainties arising from data-MC disagreement between track-related variables are considered. There is also still a 5% contribution from tracking efficiency (a global uncertainty for the p_T differential measurement). The ratio computed through (4) is shown as a function of B p_T in Figure 10. The measurement was, once again, performed within the fiducial region. The results are compared with the f_s/f_u in pp collisions, estimated from the measured $f_s/(f_u+f_d)$, using the assumption $f_s/(f_u+f_d) \sim 0.5(f_s/f_u)$. The ratio results provide evidence of an enhancement in the low to mid p_T region, indicating a possibly sizeable contribution to b-quark hadronization from recombination effects in a medium with an enhanced strangeness population.

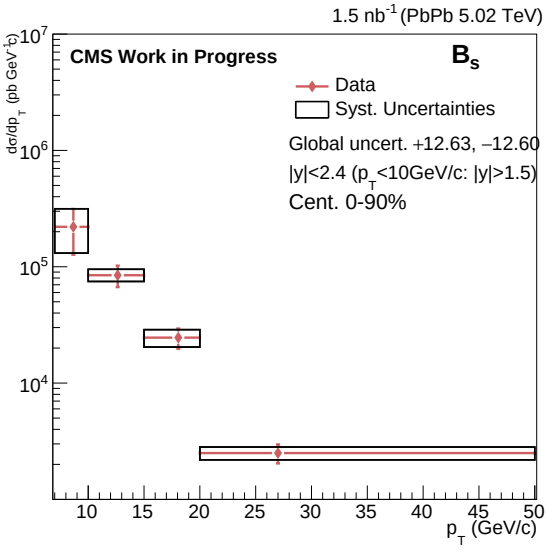

Figure 8: B_s cross section in PbPb collisions, as a function of p_T. The measurement was performed within the analysis fiducial region. The data points (represented at the weighted-average of the p_T distributions of each bin), and their respective statistical uncertainties can be seen in light red. The rectangular boxes represent the systematic uncertainties. The horizontal bars do not represent uncertainties, but the range of the p_T bin. The p_T bins range from 7 to 50 GeV/c.

The production ratios were also computed for different centrality ranges (Table 1). The dominant source of uncertainty is statistic. Figure 9 shows the B_s/B^+ production ratio, as a function of $\langle N_{part}\rangle$, corresponding to the 0-30% and 30-90% centrality classes, and estimated from Glauber Model calculations. One can see that R is higher for the centrality range of 0-30% than for centrality 30-90%. This means that for higher centrality, the production of B_s over B^+ is higher. This is expected, since for higher number of nucleon partici-

pants the strangeness content of the medium must be enhanced. The results are compared with the average fragmentation fraction ratio f_s/f_u, measured by LHCb in pp collisions [13], showing evidences of enhanced production ratio for more central collisions.

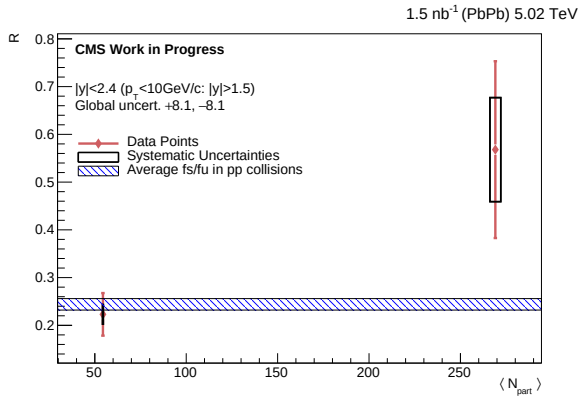

Figure 9: B_s/B^+ production ratio, as a function of $\langle N_{part} \rangle$ (corresponding to the centrality class being studied). The measurement was performed within the analysis fiducial region. The data points, and their respective statistical uncertainties can be seen in light red. The rectangular boxes represent the systematic uncertainties. The average fragmentation fraction ratio f_s/f_u, measured by LHCb in pp collisions [13] within its uncertainty is represented in blue.

The B_s cross section results were further normalised by published results of the B_s cross section measurement in pp collisions at the same center-of-mass energy. This study was done for the p_T range of 15-50 GeV/c. Figure 11 shows the resulting nuclear modification factors.

A comparison can be made with the nuclear modification results obtained from the 2015 dataset (Figure 12). The published B_s R_{AA} for the p_T of 15-50 GeV/c was $R_{AA} = 0.80 \pm 0.30$ (stat) $\pm$ 0.17 (syst) [11]. That result was compatible with values higher than unity (within systematic and statistical uncertainties), and so there was still a case to be done for enhancement in that p_T range. The result presented by this work points to an overall suppression of B_s production, in PbPb compared to pp collisions, in the mentioned, higher p_T range.

Further comparing the B_s R_{AA} here obtained with the B^+ R_{AA} previously reported [11], one can see that there is a hint of an enhancement by the QGP of B_s production relative to B^+. The outcome of this R_{AA} comparison study is accordingly compatible with the production ratio comparison with f_s/f_u also reported above. These results would be explained, as mentioned previously, by sizeable contribution of bottom quark recombination with lighter quarks in the presence of a medium with increased strangeness content.

Employing the larger dataset available, the first significant observation of the B_s signal in PbPb

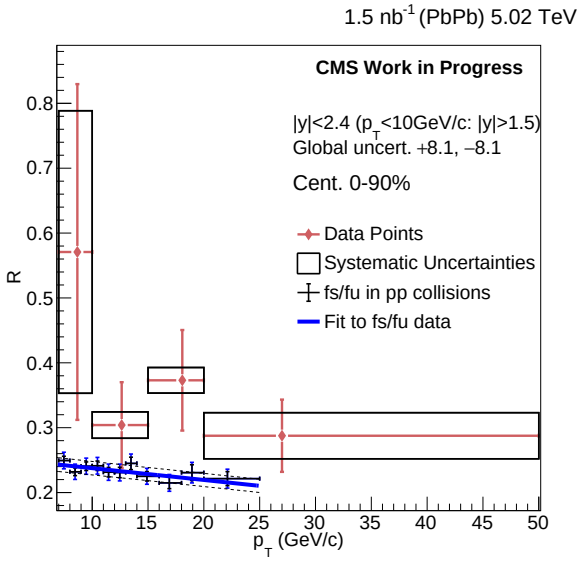

Figure 10: B_s/B^+ production ratio, as a function of p_T. The measurement was performed within the analysis fiducial region. The data points (represented at the weighted-average of the B_s p_T distributions of each bin), and their respective statistical uncertainties can be seen in light red. The rectangular boxes represent the systematic uncertainties. The horizontal bars do not represent uncertainties, but the range of the p_T bin. The p_T bins range from 7 to 50 GeV/c. The f_s/f_u in pp collisions (LHCb measurement) is also displayed, for comparison [13]. The smaller (black) error bars represent the bin-by-bin systematics of that analysis, and the blue error bars represent the global uncertainties. The resulting function from the linear fit to those data points (performed in the LHCb analysis) is superimposed, in blue. The dashed lines give the total uncertainties on the fit results.

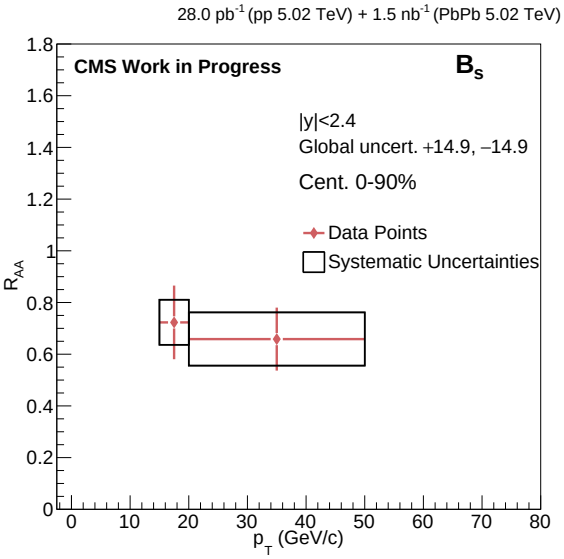

Figure 11: B_s nuclear modification factor measured in two p_T intervals, in the range 15-50 GeV/c. The cross sections measured in this work were normalised by the cross sections measured in pp collisions at the same center-of-mass energy, published by CMS [11]. The data points, and their respective statistical uncertainties can be seen in light red. The rectangular boxes represent the systematic uncertainties.

Table 1: Production ratio in different centrality ranges.

Centrality range	Production ratio	Stat. Uncertainty (%)	Syst. Uncertainty (%)
0 - 30%	0.568	32.6	9.22
30 - 90%	0.223	20.0	19.18
0 - 90%	0.415	19.2	14.83

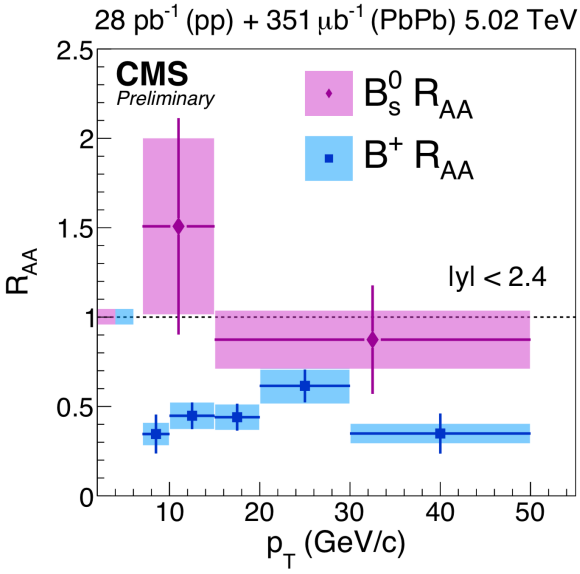

Figure 12: B_s nuclear modification factor measured in two p_T intervals, in the range 7-50 GeV/c (pink data points). This measurement was performed with the smaller 2015 dataset, with an integrated luminosity of 351 μb^{-1}. [11] Overlaid is also the B^+ nuclear modification obtained with the same dataset (blue data points). The rectangular boxes, in both cases, represent the systematic uncertainties.

collisions was achieved by this work. It was also possible to more precisely study the production of B_s relative to the B^+ in PbPb collisions, further comparing it to the fragmentation fraction ratio f_s/f_u measured in pp collisions. The production ratio is seen to increase for low to mid p_T, indicating hadronisation from recombination in the strangeness enhanced medium.

The measurement of the B_s nuclear modification factor from 15-50 GeV/c indicates overall suppression of the meson's production in the QGP medium. Further comparing that newly calculated B_s R_{AA} with the published B^+ R_{AA} there is once again the hint of medium induced enhancement.

The precision of the results here reported will benefit from increased PbPb data sets that will be collected in future LHC runs. The combined PbPb data collected during 2015 and 2018 can be used at once to obtain improved results. In particular, this will yield more precise results for the low-p_T region, where recombination effects are expected to be more pronounced. The larger overall sample could also allow for a finer kinematic and centrality binning. The B^0 meson has not been studied as part of this thesis, due to lack of simulated samples. The production ratios between B^+ and B^0 could be further used to probe bottom-quark hadronization in the QGP medium, and the effect of recombination. The nuclear modification factor measurements shall benefit from the combined PbPb samples, as well as from the larger pp reference dataset collected by CMS in 2017, at the same center-of-mass collision energy as studied in this work. Furthermore, the nuclear modification factors of all 3 mesons B^+, B_s and B^0, could be measured with greater precision by using all the PbPb and pp data collected at 5.02 TeV. More data will allow to start exploring rarer processes, and new hadrons, such as the B_c meson, allowing to probe potential effects of charm enhancement, and the X(3872), opening the window into the study of exotic spectroscopy in ion collisions. All these measurements and novel probes shall add precision to the study of energy loss, its flavour dependence, quark recombination effects, and beyond - towards an improved understanding of the primordial QGP medium.

9. Conclusions

- N - raw signal yield
- $\mathcal{A}$ - detector acceptance
- ϵ - reconstruction efficiency
- $\mathcal{B}$ - decay branching fraction
- $\mathcal{L}$ - luminosity

References

[1] W. Busza, K. Rajagopal, and W. van der Schee. Heavy Ion Collisions: The Big Picture, and the Big Questions. *Ann. Rev. Nucl. Part. Sci.*, 68:339–376, 2018.

[2] Y. L. Dokshitzer and D. E. Kharzeev. Heavy quark colorimetry of QCD matter. *Phys. Lett.*, B519:199–206, 2001.

[3] X. Dong, Y.-J. Lee, and R. Rapp. Open Heavy-Flavor Production in Heavy-Ion Collisions. 2019.

[4] V. Khachatryan et al. Charged-particle nuclear modification factors in PbPb and pPb collisions at $\sqrt{s_{\mathrm{N\,N}}} = 5.02$ TeV. *JHEP*, 04:039, 2017.

[5] V. Khachatryan et al. Measurement of the total and differential inclusive B^+ hadron cross sections in pp collisions at $\sqrt{s}$ = 13 TeV. *Phys. Lett.*, B771:435–456, 2017.

[6] V. Khachatryan, A. Sirunyan, A. Tumasyan, W. Adam, E. Asilar, T. Bergauer, J. Brandstetter, E. Brondolin, M. Dragicevic, J. Erö, and et al. The CMS trigger system. *Journal of Instrumentation*, 12(01):P01020–P01020, Jan 2017.

[7] M. L. Miller, K. Reygers, S. J. Sanders, and P. Steinberg. Glauber modeling in high energy nuclear collisions. *Ann. Rev. Nucl. Part. Sci.*, 57:205–243, 2007.

[8] M. Pivk and F. R. Le Diberder. SPlot: A Statistical tool to unfold data distributions. *Nucl. Instrum. Meth.*, A555:356–369, 2005.

[9] J. Rafelski and B. Müller. Strangeness Production in the Quark-Gluon Plasma. *Phys. Rev. Lett.*, 48:1066–1069, Apr 1982.

[10] B. P. Roe, H.-J. Yang, J. Zhu, Y. Liu, I. Stancu, and G. McGregor. Boosted decision trees, an alternative to artificial neural networks. *Nucl. Instrum. Meth.*, A543(2-3):577–584, 2005.

[11] A. M. Sirunyan et al. Measurement of $\mathrm{B}_{\mathrm{s}}^{0}$ meson production in pp and PbPb collisions at $\sqrt{s_{\mathrm{NN}}} = 5.02$ TeV. *Submitted to: Phys. Lett.*, 2018.

[12] M. Tanabashi et al. Review of Particle Physics. *Phys. Rev. D*, 98:030001, Aug 2018.

[13] The LHCb Collaboration. Measurement of b hadron fractions in 13 TeV pp collisions. *Phys. Rev. D*, 100:031102, Aug 2019.